The Astrophysical Journal, 674:L5–L8, 2008 February 10

LUMINOSITY-DEPENDENT X-RAY ACTIVE GALACTIC NUCLEUS CLUSTERING?

M. Plionis,[1,2] M. Rovilos,[1] S. Basilakos,[3] I. Georgantopoulos,[1] and F. Bauer[4]

Received 2007 August 10; accepted 2007 December 19; published 2008 January 14

ABSTRACT

We have analyzed the angular clustering of X-ray–selected active galactic nuclei (AGNs) in different flux-limited subsamples of the *Chandra* Deep Field North (CDF-N) and South (CDF-S) surveys. We find a strong dependence of the clustering strength on the subsample flux limit, a fact that explains most of the disparate clustering results of different *XMM* and *Chandra* surveys. Using Limber's equation, we find that the inverted CDF-N and CDF-S spatial clustering lengths are consistent with direct spatial clustering measures found in the literature, while at higher flux limits the clustering length increases considerably; for example, at $f_{x,\rm limit} \sim 10^{-15}$ ergs s^{-1} cm^{-2}, we obtain $r_0 \simeq 17 \pm 5$ and $18 \pm 3\ h^{-1}$ Mpc for the CDF-N and CDF-S, respectively. We show that the observed flux limit clustering trend hints toward an X-ray luminosity dependent clustering of X-ray–selected, $z \sim 1$, AGNs.

Subject headings: cosmology: observations — galaxies: active — large-scale structure of universe — quasars: general — surveys

On-line material: color figures

1. INTRODUCTION

X-ray–selected active galactic nuclei (AGNs) provide a relatively unbiased census of the AGN phenomenon, since obscured AGNs, largely missed in optical surveys, are included in such surveys. Furthermore, they can be detected out to high redshifts and thus trace the distant density fluctuations providing important constraints on supermassive black hole formation, the relation between AGN activity and dark matter (DM) halo hosts, the cosmic evolution of the AGN phenomenon (e.g., Mo & White 1996; Sheth, Mo, & Tormen 2001), and cosmological parameters and the dark energy equation of state (e.g., Basilakos & Plionis 2005, 2006; Plionis & Basilakos 2007).

Until quite recently our knowledge of X-ray AGN clustering came exclusively from analyses of *ROSAT* data ($\lesssim$3keV) (e.g., Boyle & Mo 1993; Vikhlinin & Forman 1995; Carrera et al. 1998; Akylas, Georgantopoulos, & Plionis 2000; Mullis et al. 2004). These analyses provided conflicting results on the nature of high-z AGN clustering. Vikhlinin & Forman (1995), using the angular correlation approach and inverting to infer the spatial correlation length, found a strong amplitude of $\bar{z} \sim 1$ sources ($r_0 \simeq 9\ h^{-1}$ Mpc), which translates into $r_0 \simeq 12\ h^{-1}$ Mpc for a ΛCDM cosmology and a luminosity-driven density evolution (LDDE) luminosity function (e.g., Hasinger et al. 2005). Carrera et al. (1998), however, using spectroscopic data, could not confirm such a large correlation amplitude.

With the advent of the *XMM* and *Chandra* X-ray observatories, many groups have attempted to settle this issue. Recent determinations of the high-z X-ray–selected AGN clustering, in the soft and hard bands, have provided again a multitude of conflicting results, intensifying the debate (e.g., Yang et al. 2003; Manners et al. 2003; Basilakos et al. 2004; Gilli et al. 2005; Basilakos et al 2005; Yang et al. 2006; Puccetti et al. 2006; Miyaji et al. 2007; Gandhi et al. 2006; Carrera et al. 2007).

In this Letter, we investigate these clustering differences by reanalyzing the *Chandra* Deep Field North (CDF-N) and South (CDF-S) surveys, using the Bauer et al. (2004) classification to select only AGNs in the 0.5–2 and 2–8 keV bands. To use all the available sources, and not only those having spectroscopic redshifts, we work in angular space and then invert the angular correlation function using Limber's equation. Hereafter, we will be using $h \equiv H_0/100$ km s^{-1} Mpc^{-1}.

2. THE X-RAY SOURCE CATALOGS

The 2 Ms CDF-N and 1 Ms CDF-S *Chandra* data represent the deepest observations currently available at X-ray wavelengths (Alexander et al. 2003; Giacconi et al. 2001). The CDF-N and CDF-S cover an area of 448 and 391 arcmin^2, respectively. We use the source catalogs of Alexander et al. (2003) for both CDF-N and CDF-S. The flux limits that we use for the CDF-N are 3×10^{-17} and 2×10^{-16} ergs cm^{-2} s^{-1} in the soft and hard bands, while for the CDF-S the respective values are 6×10^{-17} and 5×10^{-16} ergs cm^{-2} s^{-1}. Note that sensitivity maps were produced following the prescription of Lehmer et al. (2005); in order to produce random catalogs in a consistent manner to the source selection, we discard sources that lie below our newly determined sensitivity map threshold, at their given position. Our final CDF-N catalogs contain 383 and 263 sources in the soft (0.5–2 keV) and hard (2–8 keV) bands, respectively, out of which 304 and 255 are AGNs, according to the "pessimistic" Bauer et al. (2004) classification. The corresponding CDF-S catalogs contain 257 and 168 sources in the same bands, out of which 227 and 165 are AGNs. A number of sources (roughly half) have spectroscopic redshift determinations (mostly taken from Barger et al. 2003; Szokoly et al. 2004; Vanzella et al. 2005, 2006; Le Févre et al. 2004; Mignoli et al. 2005).

3. CORRELATION FUNCTION ANALYSIS

3.1. *The Angular Correlation*

The clustering properties of the X-ray AGNs are estimated using the two-point angular correlation function, $w(\theta)$, esti-

[1] Institute of Astronomy and Astrophysics, National Observatory of Athens, I. Metaxa & B. Pavlou, P. Penteli, 152 36 Athens, Greece.

[2] Instituto Nacional de Astrofisica, Optica y Electronica (INAOE) Apartado Postal 51 y 216, 72000 Puebla, Pue., Mexico.

[3] Academy of Athens, Research Centre for Astronomy and Applied Mathematics, Soranou Efessiou 4, 11-527 Athens, Greece.

[4] Columbia Astrophysics Laboratory, Columbia University, Pupin Physics Laboratories, 550 West 120th Street, New York, NY.

TABLE 1
INTEGRATED ANGULAR CLUSTERING SIGNAL (σ)

SAMPLE	$f_{x,\rm limit}$[a]		$f_{x,\rm limit}$[b]	
	<400″	<900″	<400″	<900″
CDF-N Soft	2.1	0.0	2.1	1.5
CDF-N Hard	3.3	2.6	6.7	5.5
CDF-S Soft	4.2	2.6	3.4	3.7
CDF-S Hard	0.3	1.3	4.1	2.7

[a] The lowest flux limit.
[b] 5×10^{-16} ergs s^{-1} cm^{-2} (soft band) and 10^{-15} ergs s^{-1} cm^{-2} (hard band).

mated using $w(\theta) = f(N_{DD}/N_{DR}) - 1$, where N_{DD} and N_{DR} are the numbers of data-data and data-random pairs, respectively, within separations θ and $\theta + d\theta$. The normalization factor is given by $f = 2N_R/(N_D - 1)$, where N_D and N_R are the total number of data and random points, respectively. The Poisson uncertainty in $w(\theta)$ is estimated as $\sigma_w = \sqrt{(1 + w(\theta))/N_{DR}}$ (Peebles 1973).

The random catalogs are produced to account for the different positional sensitivity and edge effects of the surveys. To this end, we generated 1000 Monte Carlo random realizations of the source distribution, within the CDF-N and CDF-S survey areas, by taking into account the local variations in sensitivity. We also reproduce the desired log N–log S distribution, either the Kim et al. (2007) or the one recovered directly from the CDF data (however, our results remain mostly unchanged using either of the two). Random positioned sources with fluxes lower than that corresponding to the particular position of the sensitivity map are removed from our final random catalog.

We apply the correlation analysis evaluating $w(\theta)$ in the range [5″, 900″] in 10 logarithmic intervals with $\delta \log \theta = 0.226$. We find statistically significant signals for all bands and for both CDF-N and CDF-S. As an example, we provide in Table 1 the integrated signal-to-noise ratios, given for two different flux limits and two different angular ranges. The significance appears to be low only for the CDF-S hard band, but for the lowest flux limit.

The angular correlation function for two different flux limits are shown in Figure 1, with the lines corresponding to the best-fit power-law model: $w(\theta) = (\theta_0/\theta)^{\gamma-1}$, using $\gamma = 1.8$ and the standard χ^2 minimization procedure. Note that for the CDF-N we get, at some angular separations, very low or even negative $w(\theta)$ values. These, however, are taken into account in deriving the integrated signal, presented in Table 1.

Applying our analysis for different flux-limited subsamples, we find that the clustering strength increases with increasing flux limit, in agreement with the CDF-S results of Giacconi et al (2001). In Figure 2 we plot the angular clustering scale, θ_0, derived from the power-law fit of $w(\theta)$, as a function of different sample flux limits. The trend is true for both energy bands and for both the CDF-N and CDF-S, although for the latter it is apparently stronger.

We also find that at their lowest respective flux limits, the clustering of CDF-S sources is stronger than that of CDF-N sources (more so for the soft band), in agreement with the spatial clustering analysis of Gilli et al. (2005). This difference has been attributed to cosmic variance, in the sense that there are a few large superclusters present in the CDF-S (Gilli et al. 2003). However, selecting CDF-N and CDF-S sources at the same flux limit reduces this difference, which remains strong only for the highest flux-limited subsamples (see Fig. 2).

It is worth mentioning that our results could in principle

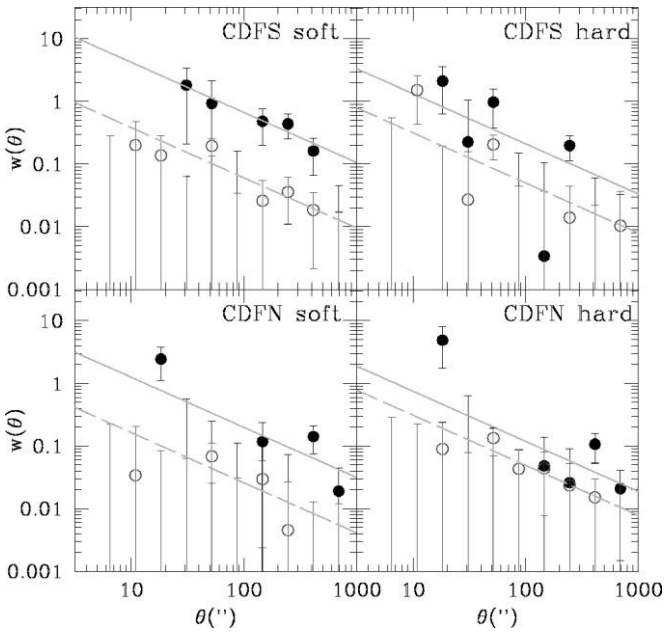

FIG. 1.—The CDF-S and CDF-N angular correlation function. The open points correspond to the overall sample and the filled points to the highest flux limit used ($f_x = 3 \times 10^{-15}$ ergs s^{-1} cm^{-2} for the soft band and $f_x = 5 \times 10^{-15}$ ergs s^{-1} cm^{-2} for the hard band). The straight lines correspond to the best power-law fit to the clustering data. Error bars correspond to 1 σ Poisson uncertainties. [*See the electronic edition of the Journal for a color version of this figure.*]

suffer from the so-called *amplification bias*, which can enhance artificially the clustering signal due to the detector's point-spread function (PSF) smoothing of source pairs with intrinsically small angular separations (see Vikhlinin & Forman 1995; Basilakos et al. 2005). However, we doubt whether this bias can significantly affect our results because at the median redshift of the sources ($z \sim 1$), the *Chandra* PSF angular size of $\sim 1''$ corresponds to a rest-frame spatial scale of only ~ 5 h^{-1} kpc (even at large off-axis angles, where the PSF size increases to $\sim 4''$, the corresponding spatial scale is only ~ 20 h^{-1} kpc). In any case, and ignoring for the moment the additional effect of the variable PSF size, the above imply that only the $w(\theta)$ of the lowest flux-limited samples could in principle be affected, but in the direction of reducing (and not inducing)

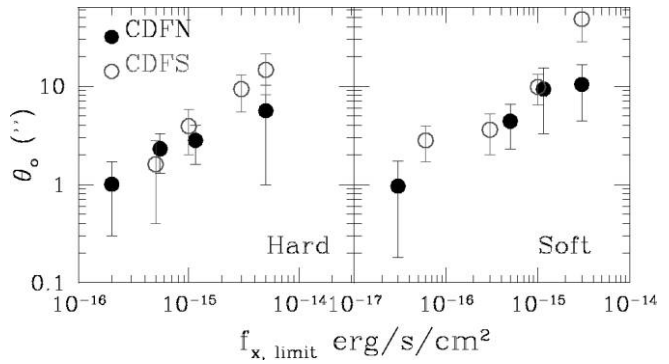

FIG. 2.—Angular clustering scale as a function of the flux limit of the different samples. The dependence of clustering strength on the flux limit is evident. The left and right panels correspond to the hard and soft bands, respectively. Filled symbols correspond to the CDF-N and open ones to the CDF-S. [*See the electronic edition of the Journal for a color version of this figure.*]

the observed θ_0-$f_{x,\rm limit}$ trend (since the uncorrected θ_0 values are, if anything, artificially larger than the true underlying one).

However, the variability of the PSF size throughout the *Chandra* field can have an additional effect and possibly enhance or even produce the observed θ_0-$f_{x,\rm limit}$ trend. To test for this, we have repeated our analysis, restricting the data to a circular area of radius 6′ around the center of the *Chandra* fields, where we expect to have a relatively small variation of the PSF size. This choice of radius was dictated as a compromise between excluding as much external area as possible but keeping enough sources ($\lesssim$50% of original) to perform the clustering analysis. The results show that indeed the θ_0-$f_{x,\rm limit}$ trend is present and qualitatively the same as when using all the sources, implying that the previously mentioned biases do not create the observed trend.

3.2. *Comparison with Other $w(\theta)$ Results*

We investigate here whether the large span of published X-ray AGN clustering results can be explained by the derived θ_0-$f_{x,\rm limit}$ trend. To this end, we attempt to take into account the different survey area curves, by estimating a characteristic flux for each survey, $f_x(\frac{1}{2}AC)$, corresponding to half its area curve (easy to estimate from the different survey published area curves).

In Figure 3 we plot the corresponding values of θ_0 (for fixed $\gamma = 1.8$) as a function of $f_x(\frac{1}{2}AC)$ (for both hard and soft bands) for the *Chandra* Large AREA Synoptic X-Ray Survey (CLASXS) (Yang et al. 2003), the *XMM*/2dF (Basilakos et al. 2004; 2005), *XMM*-COSMOS (Miyaji et al. 2007), *XMM*-ELAIS-S1 (Puccetti et al. 2006), *XMM*-LSS (Gandhi et al. 2006), and AXIS (Carrera et al. 2007) surveys. With the exception of the Yang et al. (2003) and the Carrera et al. (2007) hard-band results, the rest are consistent with the general flux-dependent trend. Note also that Gandhi et al. (2006) do not find any significant clustering of their hard-band sources. Of course, cosmic variance is also at work (as evidenced also by the clustering differences between the CDF-N and CDF-S; see Fig. 2 and Gilli et al. 2005) which should be responsible for the observed scatter around the main trend (see also Stewart et al. 2007).

We would like to stress that the CDF surveys have a large flux dynamical range, which is necessary in order to investigate the $f_{x,\rm limit}$-θ_0 correlation. This is probably why this effect has not been clearly detected in other surveys, although recently a weak such effect was found also in the CLASXS survey (Yang et al. 2006).

3.3. *The Spatial Correlation Length Using $w(\theta)$*

We can use Limber's equation to invert the angular clustering and derive the corresponding spatial clustering length, r_0 (e.g., Peebles 1993). To do so, it is necessary to model the spatial correlation function as a power law and to assume a clustering evolution model, which we take to be that of constant clustering in comoving coordinates (e.g., de Zotti et al. 1990; Kundić 1997). For the inversion to be possible it is necessary to know the X-ray source redshift distribution, which can be determined by integrating the corresponding X-ray source luminosity function above the minimum luminosity that corresponds to the particular flux limit used. To this end, we use the Hasinger et al. (2005) and La Franca et al. (2005) LDDE luminosity functions for the soft and hard bands, respectively.

We perform the above inversion in the framework of the *concordance* ΛCDM cosmological model ($\Omega_m = 1 - \Omega_\Lambda =$ 0.3). The resulting values of the spatial clustering lengths, r_0, show the same dependence on flux limits, as in Figure 2.

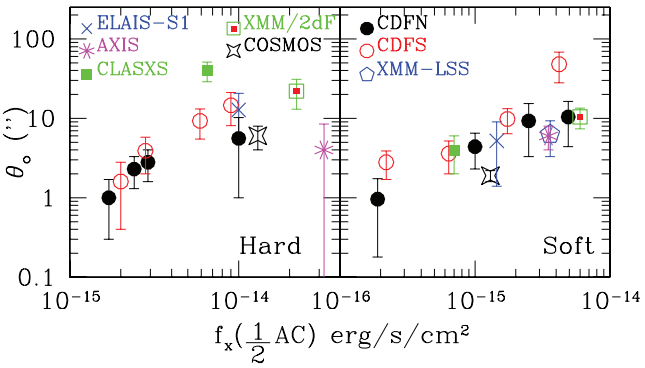

FIG. 3.—Angular correlation scale, θ_0, as a function of different survey characteristic flux, defined as that corresponding to half the respective survey area curves. Most results appear to be consistent with the clustering flux limit dependence, found from the CDF-N and CDF-S. Note that in the left panel we plot the 4.5–10 keV results of Miyaji et al. (2007). Error bars correspond to 1 σ Poisson uncertainties.

We can compare our results with direct determinations of the spatial correlation function from Gilli et al. (2005), who used a smaller (~50%) spectroscopic sample from the CDF-N and CDF-S. They found a significant difference between the CDF-S and CDF-N clustering, with $r_0 = 10.3 \pm 1.7\ h^{-1}$ Mpc and $r_0 = 5.5 \pm 0.6\ h^{-1}$ Mpc, respectively (note also that the corresponding slopes were quite shallow, roughly $\gamma \simeq$ 1.4–1.5). Since Gilli et al. used sources from the full (0.5–8 keV) band, we compare their results with our soft-band results, which dominate the total-band sources. This comparison is possible, because as we have verified using a Kolmogorov-Smirnov test, the flux distributions of the subsamples that have spectroscopic data are statistically equivalent with those of the whole samples. Our inverted clustering lengths for the lowest flux limit used are $r_0 = 10.3 \pm 2\ h^{-1}$ Mpc and $r_0 = 6.4 \pm 2.5\ h^{-1}$ Mpc (fixing $\gamma = 1.8$) for the CDF-S and CDF-N, respectively, in good agreement with the Gilli et al. (2005) direct three-dimensional determination.[5] Our values can be also compared with the recalculation of the CDF-N spatial clustering by Yang et al. (2006), who find $r_0 \simeq 4.1 \pm 1.1\ h^{-1}$ Mpc.

We return now to the strong trend between θ_0 (or the corresponding r_0) and the sample flux limit (see Figs. 2 and 3), which could be due to two possible effects (or the combination of both). Either the different flux limits correspond to different intrinsic luminosities, i.e., a luminosity-clustering dependence (see also hints in the CLASXS and CDF-N based Yang et al. 2006 results; while for optical data, see Porciani & Norberg 2006) or a redshift-dependent effect (i.e., different flux limits correspond to different redshifts traced). Using the sources that have spectroscopic redshift determinations, we have derived their intrinsic luminosities, in each respective band, from their count rates using a spectral index $\Gamma = 1.9$ and the *concordance* ΛCDM cosmology. We have also applied an absorption correction by assuming a power-law X-ray spectrum with an intrinsic $\Gamma = 1.9$, obscured by an optimum column density to reproduce the observed hardness ratio. We then derive, for each flux limit used, the median redshift and median luminosity of the corresponding subsample. We find relatively small varia-

[5] Leaving both r_0 and γ as free parameters in the fit, we obtain γ-values quite near their nominal value ($\gamma \sim 1.6$–1.8).

tions and no monotonic change of the median redshift with subsample flux limit. For example, the median spectroscopic redshifts for the soft and hard bands, at the lowest flux limit used, are $\bar{z} \sim 0.8$ and ~0.95, respectively, while the mean variations between the different flux limits used are $\langle \delta z/z \rangle \simeq -0.11$ and -0.03 for the CDF-N and $\langle \delta z/z \rangle \simeq -0.27$ and 0.05 for the CDF-S soft and hard bands, respectively. The large redshift variation of the soft-band CDF-S data should be attributed to the presence of a few superclusters at $z \sim 0.7$ (see Gilli et al. 2003).

In Figure 4 we present the correlation between the subsample median X-ray luminosity and the corresponding subsample clustering length, as provided by Limber's inversion. Although the CDF luminosity dynamical range is limited, it is evident that the median X-ray luminosity systematically increases with increasing sample flux limit, and it is correlated to r_0 (as expected from Fig. 2). It should be noted that the correlation length of the highest-flux–limited CDF-S soft-band subsample is by far the largest ever found ($\sim 30\ h^{-1}$ Mpc), but one has to keep in mind that the CDF-S appears not to be a typical field, as discussed earlier (see Gilli et al. 2003). The CDF-N high-flux results appear to converge to a value of $r_0 \sim 18\ h^{-1}$ Mpc, similar to that of some other surveys (e.g., Basilakos et al. 2004, 2005; Puccetti et al. 2006).

We therefore conclude not only that are there indications for a luminosity dependent clustering of X-ray–selected high-z AGNs but also that they are significantly more clustered than their lower-z counterparts, which have $r_0 \sim 7$–$8\ h^{-1}$ Mpc (e.g., Akylas et al. 2000; Mullis et al. 2004). This is a clear indication of a strong bias evolution (e.g., Basilakos, Plionis, & Ragone-Figueroa 2008).

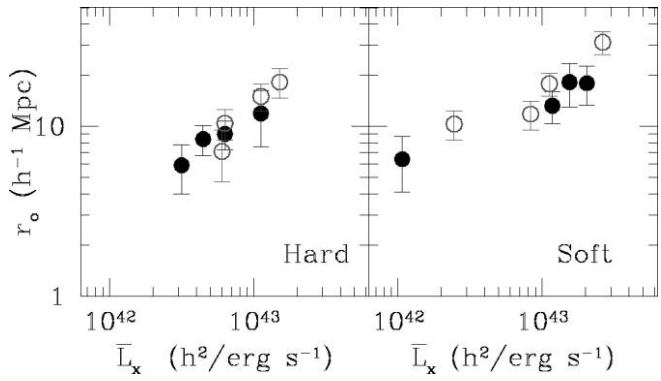

FIG. 4.—Correlation between the clustering length, r_0, and the median intrinsic X-ray luminosity of each subsample. The left and right panels correspond to the hard and soft bands, respectively. Filled symbols correspond to the CDF-N and open ones to the CDF-S. [*See the electronic edition of the Journal for a color version of this figure.*]

4. CONCLUSIONS

We have analyzed the angular clustering of the CDF-N and CDF-S X-ray AGNs and find the following:

1. A dependence of the angular clustering strength on the sample flux limit. Most *XMM* and *Chandra* clustering analyses provide results that are consistent with the observed trend, a fact that appears to lift the confusion that arose from the apparent differences in their respective clustering lengths.

2. Within the concordance cosmological model, the comoving clustering evolution model, and the LDDE luminosity function, our angular clustering results are in good agreement with direct estimations of the CDF-N and CDF-S spatial clustering, which are based however on roughly half the total number of sources for which spectroscopic data were available.

3. The apparent correlation between clustering strength and sample flux limit transforms into a correlation between clustering strength and intrinsic X-ray luminosity, since no significant redshift-dependent trend was found.

REFERENCES

Akylas, A., Georgantopoulos, I., & Plionis, M. 2000, MNRAS, 318, 1036
Alexander, D. M., et al. 2003, AJ, 126, 539
Barger, A. J., et al. 2003, AJ, 126, 632
Basilakos, S., Georgakakis, A., Plionis, M., & Georgantopoulos, I. 2004, ApJ, 607, L79
Basilakos, S., & Plionis, M. 2005, MNRAS, 360, L35
———. 2006, ApJ, 650, L1
Basilakos, S., Plionis, M., Georgantopoulos, I., & Georgakakis, A. 2005, MNRAS, 356, 183
Basilakos, S., Plionis, M., & Ragone-Figueroa, C. 2008, ApJ, in press
Bauer, F. E., Alexander, D. M., Brandt, W. N., Schneider, D. P., Treister, E., Hornschemeier, A. E., & Garmire, G. P. 2004, AJ, 128, 2048
Boyle, B. J., & Mo, H. J. 1993, MNRAS, 260, 925
Carrera, F. J., Barcons, X., Fabian, A. C., Hasinger, G., Mason, K. O., McMahon, R. G., Mittaz, J. P. D., & Page, M. J. 1998, MNRAS, 299, 229
Carrera, F. J., et al. 2007, A&A, 469, 27
de Zotti, G., Persic, M., Franceschini, A., Danese, L., Palumbo, G. G. C., Boldt, E. A., & Marshall, F. E. 1990, ApJ, 351, 22
Gandhi, P., et al. 2006, A&A, 457, 393
Giacconi, R., et al. 2001, ApJ, 551, 624
Gilli, R., et al. 2003, ApJ, 592, 721
———. 2005, A&A, 430, 811
Hasinger, G., Miyaji, T., & Schmidt, M. 2005, A&A, 441, 417
Kim, M., Wilkes, B. J., Kim, D-W., Green, P. J., Barkhouse, W. A., Lee, M. G., Silverman, J. D., & Tananbaum, H. D. 2007, ApJ, 659, 29
Kundić, T. 1997, ApJ, 482, 631
La Franca, F., et al. 2005, ApJ, 635, 864
Le Févre, O., et al. 2004, A&A, 428, 1043
Lehmer, B. D., et al. 2005, ApJS, 161, 21
Manners, J. C., et al. 2003, MNRAS, 343, 293
Mignoli, M., et al. 2005, A&A, 437, 883
Miyaji, T., et al. 2007, ApJS, 172, 396
Mo, H. J., & White, S. D. M 1996, MNRAS, 282, 347
Mullis, C. R., Henry, J. P., Gioia, I. M., Böhringer, H., Briel, U. G., Voges, W., & Huchra, J. P. 2004, ApJ, 617, 192
Peebles, P. J. E. 1973, ApJ, 185, 413
———. 1993, Principles of Physical Cosmology (Princeton: Princeton Univ. Press)
Plionis, M., & Basilakos, S. 2007, in Proc. 6th International Workshop on the Identification of Dark Matter, Rhodes, Greece (astro-ph/0701696)
Porciani, C., & Norberg, P. 2006, MNRAS, 371, 1824
Puccetti, S., et al. 2006, A&A, 457, 501
Sheth, R. K., Mo, H. J., & Tormen, G. 2001, MNRAS, 323, 1
Stewart, G. C. 2007, talk presented at X-Ray Surveys: Evolution of Accretion, Star-Formation and the Large-Scale Structure, Rodos Island, Greece (http://www.astro.noa.gr/xray07/rodos-talks/)
Szokoly, G. P., et al. 2004, ApJS, 155, 271
Vanzella, E., et al. 2005, A&A, 434, 53
———. 2006, A&A, 454, 423
Vikhlinin, A., & Forman, W. 1995, ApJ, 455, L109
Yang, Y., Mushotzky, R. F., Barger, A. J., & Cowie, L. L. 2006, ApJ, 645, 68
Yang, Y., Mushotzky, R. F., Barger, A. J., Cowie, L. L., Sanders, D. B., & Steffen, A. T. 2003, ApJ, 585, L85